The EMBO Journal Vol. 19 No. 13 pp. 3496–3506, 2000

Limited overlapping roles of P15^{INK4b} and P18^{INK4c} cell cycle inhibitors in proliferation and tumorigenesis

Esther Latres[1,2], Marcos Malumbres[1,3], Rocío Sotillo[1,3], Javier Martín[1,3], Sagrario Ortega[1,3], Juan Martín-Caballero[3], Juana María Flores[4], Carlos Cordón-Cardo[5] and Mariano Barbacid[1,3,6]

[1]Molecular Oncology Program, Centro Nacional de Investigaciones Oncológicas Carlos III, 28220 Majadahonda, [3]Centro Nacional de Biotecnología, CSIC, Campus Universidad Autónoma and [4]Departamento de Patología Animal II, Facultad de Veterinaria, Universidad Complutense de Madrid, 28049 Madrid, Spain and [5]Department of Pathology, Memorial Sloan-Kettering Cancer Centre, New York, NY 10021, USA

[2]Present address: Department of Pathology, New York University Medical Center, New York, NY 10016, USA

[6]Corresponding author
e-mail: mariano.barbacid@cnio.es

Entry of quiescent cells into the cell cycle is driven by the cyclin D-dependent kinases Cdk4 and Cdk6. These kinases are negatively regulated by the INK4 cell cycle inhibitors. We report the generation of mice defective in *P15^{INK4b}* and *P18^{INK4c}*. Ablation of these genes, either alone or in combination, does not abrogate cell contact inhibition or senescence of mouse embryo fibroblasts in culture. However, loss of P15^{INK4b}, but not of P18^{INK4c}, confers proliferative advantage to these cells and makes them more sensitive to transformation by H-*ras* oncogenes. *In vivo*, ablation of *P15^{INK4b}* and *P18^{INK4c}* genes results in lymphoproliferative disorders and tumor formation. Mice lacking P18^{INK4c} have deregulated epithelial cell growth leading to the formation of cysts, mostly in the cortical region of the kidneys and the mammary epithelium. Loss of both P15^{INK4b} and P18^{INK4c} does not result in significantly distinct phenotypic manifestations except for the appearance of cysts in additional tissues. These results indicate that P15^{INK4b} and P18^{IKN4c} are tumor suppressor proteins that act in different cellular lineages and/or pathways with limited compensatory roles.

Keywords: cell cycle inhibitors/cyclin D-dependent Cdk/cysts/lymphoproliferative disorders/tumors

Introduction

Cellular proliferation follows an orderly progression through the cell cycle, driven by protein complexes composed of cyclins and cyclin-dependent kinases (Cdks) (reviewed in Morgan, 1995; Wuarin and Nurse, 1996). Progression through the G_1–S transition requires the activity of at least two different types of kinases, cyclin D–Cdk4/6 and cyclin E/A–Cdk2. The activity of these kinases is regulated differentially by the INK4 and Cip/Kip families of cell cycle inhibitors (reviewed in Sherr and Roberts, 1999). The members of the Cip/Kip family, p21^{Cip1}, p27^{Kip1} and p57^{Kip2}, can associate with and inactivate cyclin E–Cdk2 and cyclin A–Cdk2 complexes. In contrast, their association with cyclin D–Cdk4 or cyclin D–Cdk6 complexes appears to have a stimulatory effect (Soos *et al*., 1996; Blain *et al*., 1997; LaBaer *et al*., 1997; Cheng *et al*., 1999). Binding of Cip/Kip proteins to cyclin D–Cdk4/6 kinases also prevents their interaction with cyclin E/A–Cdk2, thus facilitating the role of these kinases in completing the G_1 phase of the cell cycle and initiating DNA synthesis (Sherr and Roberts, 1999). On the other hand, the members of the INK4 family, P16^{INK4a}, P15^{INK4b}, P18^{INK4c} and P19^{INK4d}, specifically target the Cdk4 and Cdk6 kinases, inhibiting their catalytic activity by preventing their binding to their regulatory cyclin D subunits (Sherr and Roberts, 1999).

The role of the INK4 proteins in controlling cell proliferation has been well illustrated. Synthesis of INK4 proteins, especially during the G_1 interval, is followed by cell arrest and differentiation in some cell lineages. For instance, P15^{INK4b} is down-regulated during mitogenic activation of resting lymphocytes, suggesting that this protein is functionally important in T-lymphocyte development (Lois *et al*., 1995). P15^{INK4b} has also been shown to be an important effector of transforming growth factor-β (TGF-β) signaling (Hannon and Beach, 1994; Reynisdóttir *et al*., 1995). P18^{INK4c} expression increases dramatically during terminal differentiation of mouse myoblasts (C2C12 cells), mouse adipocytes (3T3-L1 cells) and human IgG-bearing B-lymphoblastoid cells (Franklin *et al*., 1996; Morse *et al*., 1997; Phelps and Xiong, 1998). *In vivo*, P18^{INK4c} expression also correlates with terminal differentiation of developing tissues such as muscle, lung, liver, thymus and eye lens (Zindy *et al*., 1997b; Phelps *et al*., 1998). More recently, Franklin *et al*. (1998) have shown that mice lacking P18^{INK4c} display widespread organomegaly. Moreover, their T and B lymphocytes have a higher proliferative rate upon mitogenic stimulation, suggesting a role for P18^{INK4c} in maintaining cellular homeostasis and proliferation.

The role of P15^{INK4b} in tumorigenesis remains to be well defined. Although the *P15^{INK4b}* locus is often deleted in human tumors, its deletion is concomitant with that of the well characterized INK4a/ARF locus (Stone *et al*., 1995). In some cases, however, loss of *P15^{INK4b}* has been observed with retention and expression of *P16^{INK4a}* (Glendening *et al*., 1995). More recently, it was found that inhibition of *P15^{INK4b}* expression by hypermethylation appears to be a common event in human lymphoid tumors (Herman *et al*., 1996) and in mouse T-cell lymphomas (Malumbres *et al*., 1997). The human *P18^{INK4c}* gene is located in chromosome 1p32, a region frequently altered in a variety of tumors. Yet

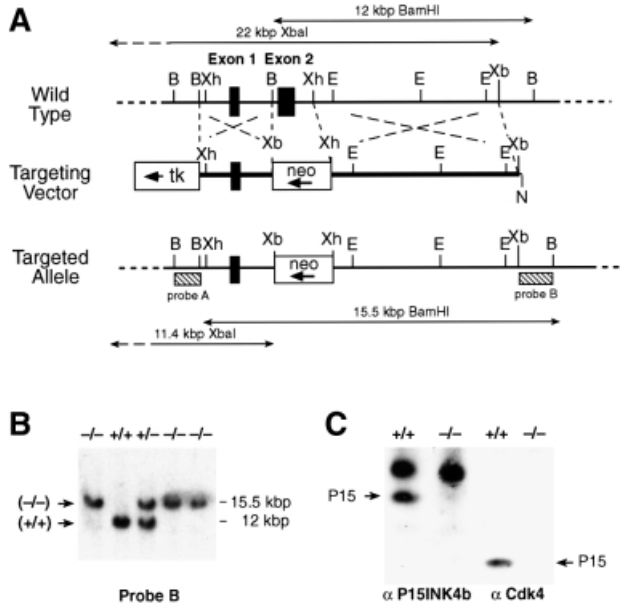

Fig. 1. Generation of *P15^{INK4b}* (–/–) mutant mice. (**A**) Schematic diagram of the targeting strategy. Top: partial restriction map of wild-type 129/Sv genomic DNA encompassing the two coding exons of the *P15^{INK4b}* locus (filled boxes) (B, *Bam*HI; E, *Eco*RI; EV, *Eco*RV; N, *Not*I; Xb, *Xba*I; Xh, *Xho*I). Middle: the targeting vector, pEL14, contains the PGK-*neo* (open box, neo) and PGK-thymidine kinase (open box, tk) cassettes. The arrows indicates the direction of transcription. Bottom: schematic diagram of the predicted targeting allele resulting from a homologous recombination event between wild-type DNA and the targeting vector. Sequences used for Southern blot analysis of recombinant ES cell clones (probes A and B) are indicated by stippled boxes. Probe A recognizes *Xba*I DNA fragments of 22 kbp (wild-type allele) and 11.4 kbp (targeted allele). Probe B detects *Bam*HI DNA fragments of 12 kbp (wild-type allele) and 15.5 kbp (targeted allele). (**B**) Southern blot analysis of mouse tail DNA isolated from newborn mice derived from crosses between *P15^{INK4b}* (+/–) mice and hybridized to probe B. The migration of the *Bam*HI DNA fragments derived from wild-type (+/+) and targeted (–/–) alleles is indicated. The corresponding genotype of each mouse is indicated on top. (**C**) Left: immunoprecipitation of MEFs derived from wild-type (+/+) or P15^{INK4b} (–/–) embryos with anti-P15^{INK4b} antibodies. Right: western blot analysis of Cdk4 immunoprecipitates with anti-P15^{INK4b} antibodies. The migration of the P15^{INK4b} protein is indicated by arrows.

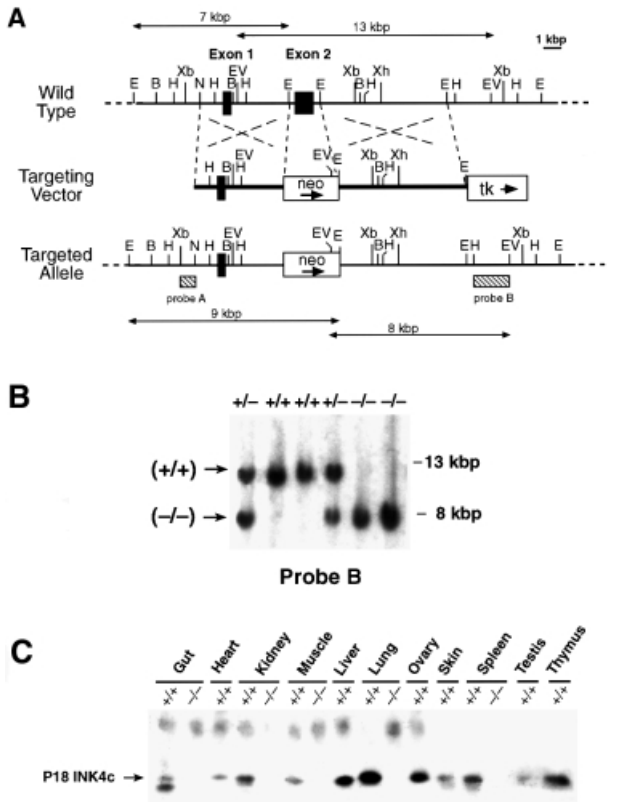

Fig. 2. Generation of *P18^{INK4c}* (–/–) mice. (**A**) Targeting strategy. Top: partial restriction map of wild-type 129/Sv genomic DNA encompassing the two coding exons (filled boxes) of the *P18^{INK4c}* gene (B, *Bam*HI; E, *Eco*RI; EV, *Eco*RV; H, *Hin*dIII; N, *Not*I; Xa, *Xba*I; Xh, *Xho*I). Middle: the targeting vector, pEL32, contains the PGK-*neo* (open box, neo) and PGK-thymidine kinase (open box, tk) cassettes. The PGK-*neo* cassette has replaced 1.4 kbp of *P18^{INK4c}* genomic sequences that encompass the entire second exon (E2). The arrows indicate the direction of transcription. Bottom: schematic diagram of the predicted structure of a targeted allele resulting from homologous recombination between wild-type sequences and the targeting vector. Sequences used for Southern blot analysis of recombinant ES cell clones (probes A and B) are indicated by stippled boxes. Probe A recognizes *Eco*RV DNA fragments of 13 kbp (wild-type allele) and 8 kbp (targeted allele). Probe B detects *Eco*RI DNA fragments of 7 kbp (wild-type allele) and 9 kbp (targeted allele). (**B**) Southern blot analysis of mouse tail DNA derived from crosses between *P18^{INK4c}* (+/–) mice using probe B. The migration of the *Eco*RV DNA fragments is indicated by arrows. The corresponding genotype of each mouse is indicated on top. (**C**) Immunoprecipitation followed by western blot analysis of tissues derived from 3-month-old *P18^{INK4c}* (+/+) and (–/–) mice. The migration of the P18^{INK4c} protein is indicated by an arrow.

this locus does not appear to be mutated in human cancer, since no mutations have been observed in >820 tumors (of various types) examined by a variety of laboratories (see, for example, Miller *et al*., 1996; Otsuki *et al*., 1996; Rusin *et al*., 1996; Hatta *et al*., 1997). In mice, ablation of the *P18^{INK4c}* locus results in the frequent development of pituitary adenomas (Franklin *et al*., 1998; this report) as well as in other types of neoplasias such as pheochromocytomas and testicular tumors (this report). These observations establish *P18^{INK4c}* as a tumor suppressor gene, at least in mice.

In the present study, we have utilized gene-targeting techniques to generate three strains of mice lacking the *P15^{INK4b}* and *P18^{INK4c}* genes alone or in combination in order to study the roles of these genes *in vivo* as well as their compensatory effects during normal mouse development and tumorigenesis.

Results

Mice lacking P15^{INK4b} and P18^{INK4c} proteins are viable and fertile

Gene-targeted disruption of the *P15^{INK4b}* (Figure 1A) and *P18^{INK4c}* (Figure 2A) loci was carried out as described in Materials and methods by eliminating their respective second coding exons (amino acid residues 44–130 in P15^{INK4b} and 43–168 in P18^{INK4c}). As illustrated in Figures 1C and 2C, these mutations result in complete loss of P15^{INK4b} and P18^{INK4c} expression, respectively. *P15^{INK4b}* (–/–) and *P18^{INK4c}* (–/–) mice are born at the expected Mendelian ratios, are fertile and do not exhibit gross morphological or behavioral abnormalities. In agreement with a previous report (Franklin *et al*., 1998),

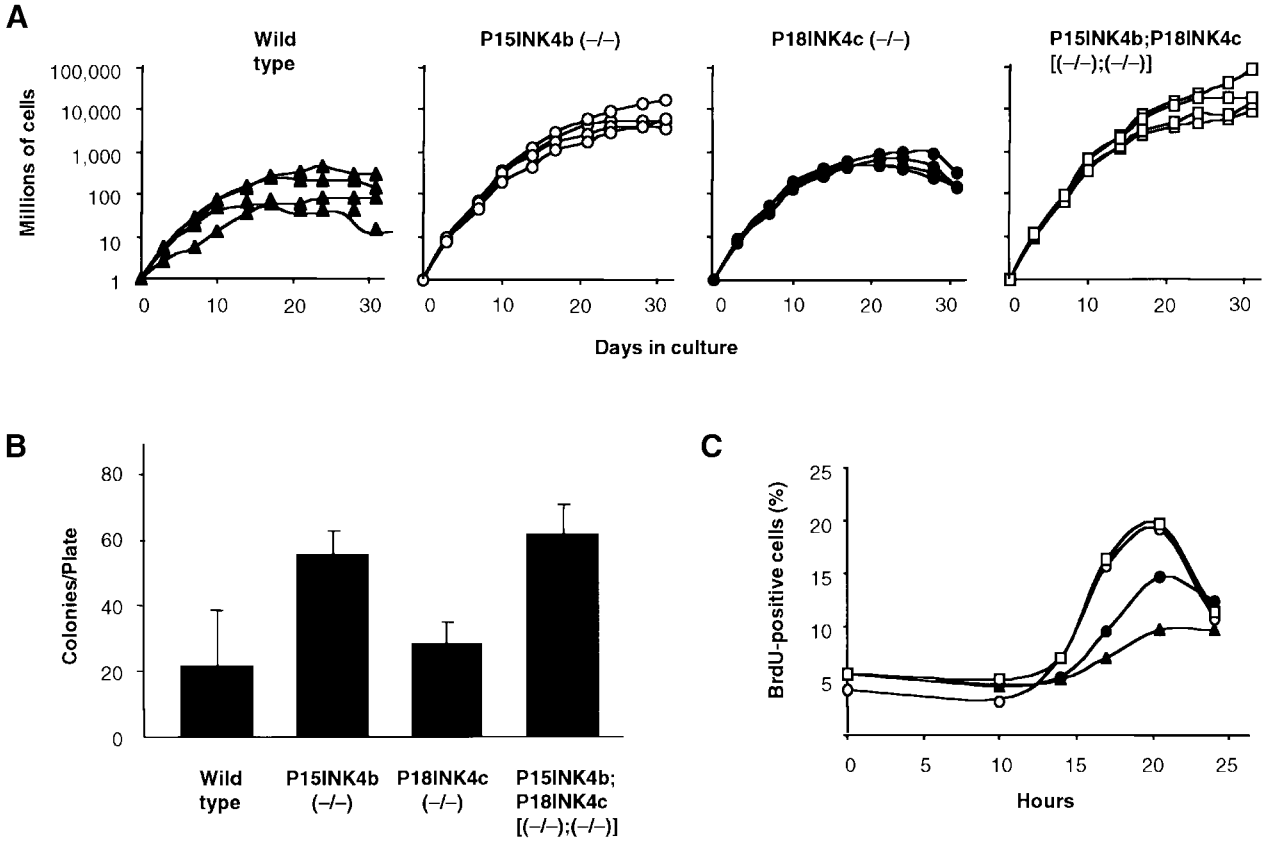

Fig. 3. Growth properties of MEFs derived from P15^{INK4}, P18^{INK4c} and P15^{INK4b};P18^{INK4c} mutant mice. (**A**) Growth curves: four independent cultures of early passage (P2) wild type (filled triangles); *P15*^{INK4b} (–/–) (open circles); *P18*^{INK4c} (–/–) (filled circles) and *P15*^{INK4b};*P18*^{INK4c} [(–/–);(–/–)] (open squares) MEFs were cultured using a standard 3T3 protocol. (**B**) Plating efficiency: 2000 cells were seeded in a 10 cm plate and colonies scored after 2 weeks in culture. (**C**) Re-entry into S phase after serum deprivation: MEFs were starved in 0.1% FBS for 48 h prior to incubation with 10% FBS (0 h) for the indicated lengths of time in the presence of BrdU. Symbols are as described in (A).

P18^{INK4c} (–/–) mice are larger than their wild-type littermates. However, the mice generated in our laboratory do not exceed the weight of wild-type mice by >20% (versus up to 45% reported by Franklin and co-workers). These quantitative differences are likely to be due to the different genetic background of the mice used to propagate the mutated allele (B6D2 versus C57BL/6).

To generate *P15*^{INK4b};*P18*^{INK4c} [(–/–);(–/–)] double mutant mice, we set up the appropriate matings between the single knockout strains. Although unknown to us at the time, the *P15*^{INK4b} and *P18*^{INK4c} loci only map 18 cM apart in mouse chromosome 4 (Zhang *et al.*, 1998). As a consequence, none of the 96 offspring mice born from crosses between *P15*^{INK4b};*P18*^{INK4c} [(+/–);(+/–)] double heterozygous animals turned out to be the expected double null mice. Fortunately, these crosses resulted in a few *P15*^{INK4b};*P18*^{INK4c} [(–/–);(+/–)] mice that, upon mating, yielded mice with the desired *P15*^{INK4b};*P18*^{INK4c} [(–/–);(–/–)] genotype at the expected Mendelian ratios. These double knockout animals are also fertile and do not exhibit obvious morphological or behavioral abnormalities. These results indicate that P15^{INK4b} and P18^{INK4c} are not essential proteins nor do they play major compensatory roles. Interestingly, the size (by weight) of these mutant mice, albeit larger than that of wild-type animals, appears to be slightly smaller (by ~5%) than that of the single *P18*^{INK4c} null mice.

Growth properties of P15^{INK4b} *(–/–) and P18*^{INK4c} *(–/–) MEFs*

Mouse embryo fibroblasts (MEFs) lacking either P15^{INK4b} or P18^{INK4c} proteins show contact inhibition and undergo senescence. However, *P15*^{INK4b} (–/–), but not *P18*^{INK4c} (–/–) MEFs display a higher proliferation rate and plating efficiency than those derived from wild-type embryos (Figure 3A and B). Surprisingly, MEFs lacking both P15^{INK4b} and P18^{INK4c} proteins behave very similarly to MEFs lacking only P15^{INK4b}, suggesting that P18^{INK4c} does not play a significant role in controlling MEF proliferation, in spite of being expressed at levels similar to P15^{INK4b} (data not shown). The ability of these mutant MEFs to enter the cell cycle after serum deprivation was also measured. As illustrated in Figure 3C, MEFs lacking P15^{INK4b}, regardless of whether they express P18^{INK4c} or not, reach the S phase more efficiently than either wild-type or P18^{INK4c}-defective MEFs. The slight increase in bromodeoxyuridine (BrdU)-positive cells suggests a limited role for P18^{INK4c} in controlling G_1–S progression in these cells (Figure 3C).

Next, we investigated whether these mutant MEFs were susceptible to transformation by *ras* and/or *myc* oncogenes. As illustrated in Figure 4, loss of P15^{INK4b}, but not of P18^{INK4c} expression results in increased susceptibility to transformation by a human H-*ras* oncogene driven by its own promoter. Co-transformation with H-*ras* and c-*myc*

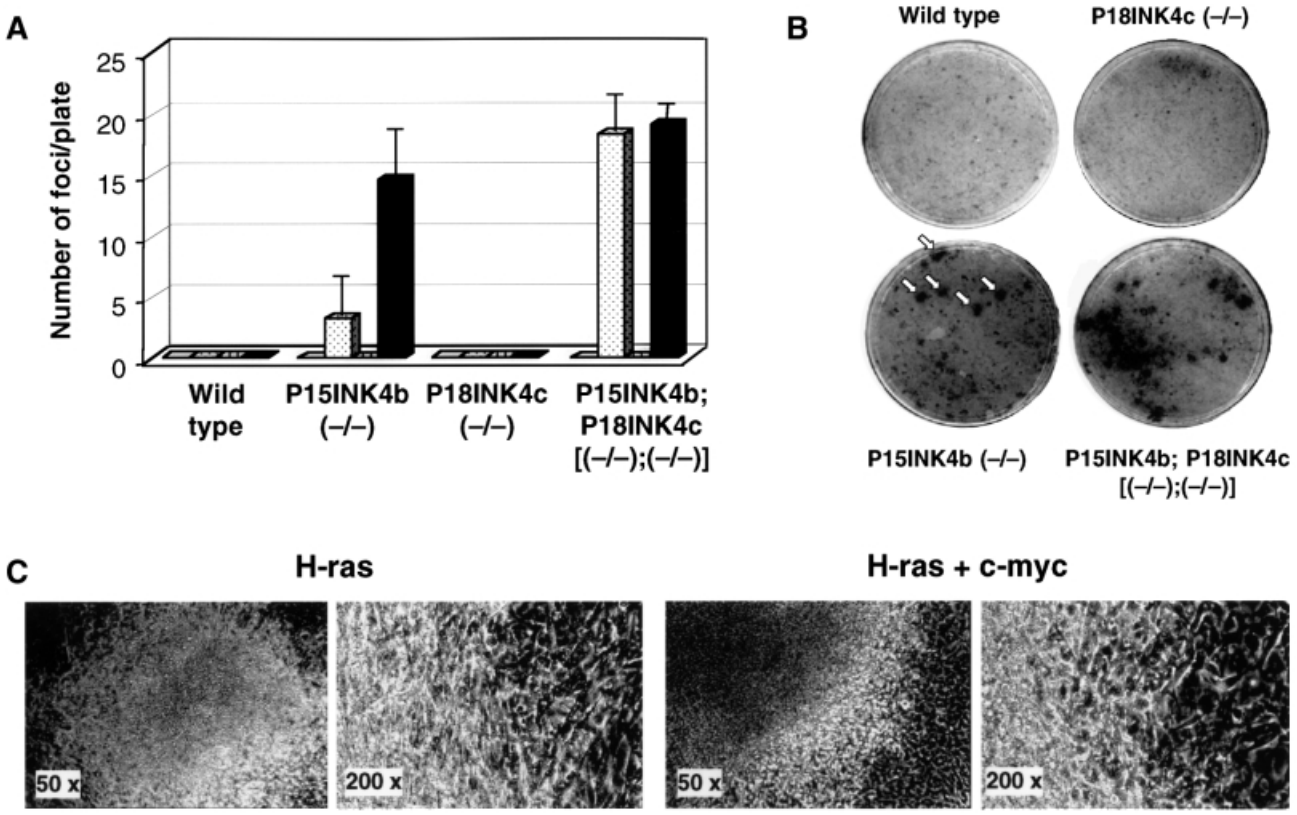

Fig. 4. Morphological transformation of mutant MEFs by H-*ras* and c-*myc* oncogenes. (**A**) The histogram shows the average number of foci per 10 cm plate and the standard deviation obtained by transfection of MEFs derived from wild-type; *P15*^{INK4b} (–/–); *P18*^{INK4c} (–/–) and *P15*^{INK4b};*P18*^{INK4c} [(–/–);(–/–)] embryos with an empty vector (open box); a plasmid containing a human H-*ras* oncogene (dotted box); a plasmid containing an SV40-driven mouse c-*myc* oncogene (stippled box); or a combination of each of these oncogene-containing plasmids (filled box). The results shown are the average of at least four separate experiments carried out with MEF cultures derived from at least five different embryos for each genotype. (**B**) A representative experiment in which MEFs derived from the indicated embryos were transfected with a plasmid containing the H-*ras* oncogene. Plates were stained with methylene blue after 15 days in culture. (**C**) Morphological appearance of representative foci obtained in the transfection of P15^{INK4b}-deficient MEFs with plasmids expressing H-*ras* alone (left) or both H-*ras* and c-*myc* (right).

oncogenes (the latter driven by the SV40 promoter) results in a significant increase (4- to 5-fold) in the number of foci of morphologically transformed cells (Figure 4A). Cells derived from most of these foci display limited proliferating properties upon continuous passage. Indeed, only cells derived from a small number of foci grew well in culture and formed colonies in soft agar (data not shown). Double mutant MEFs lacking P15^{INK4b} and P18^{INK4c} are equally sensitive to transformation by H-*ras* oncogenes alone or in combination with c-*myc* (Figure 4A). Therefore, it is possible that lack of P18^{INK4c} expression releases cells from a growth constraint similar to that induced by expression of the c-*myc* oncogene.

P15INK4b is not required for TGF-β-mediated arrest

Previous studies have indicated that TGF-β-mediated growth arrest results in the rapid induction (up to 30-fold) of P15^{INK4b} in human keratinocytes (Hannon and Beach, 1994). Yet, TGF-β may induce cell cycle arrest by mechanisms other than P15^{INK4b} induction. For instance, Iavarone and Massague (1997) have reported that TGF-β down-regulates expression of the tyrosine phosphatase Cdc25A in tumor cells lacking P15^{INK4b}. Likewise, TGF-β induces cell growth arrest of human HepG2 hepatocellular carcinoma cells by inhibiting a Cdk2-activating kinase (Nagahara *et al*., 1999). To determine the effect of TGF-β on *P15*^{INK4b} (–/–) primary mouse keratinocytes, we exposed cultures to different concentrations of TGF-β for 24 h. Thymidine incorporation analysis revealed that primary keratinocytes derived from wild-type or mutant mice are equally responsive to growth inhibition by TGF-β (Figure 5A). Similar results were obtained with cultures of MEFs, although the overall inhibition rate was lower than that observed in keratinocytes (data not shown).

Next, we investigated whether the response of these cells to TGF-β might be a consequence of compensatory mechanisms by other cell cycle inhibitors such as P16^{INK4a}, P21^{Cip1} and P27^{Kip1}. As illustrated in Figure 5B, the levels of expression of these proteins do not appear to be significantly affected by the absence of P15^{INK4b}. We also examined whether the inhibitory growth effect of TGF-β in P15^{INK4b} (–/–) MEFs might be mediated by increased binding of any of these inhibitors to Cdk4. Only P16^{INK4a} appeared to be bound to Cdk4 in greater amounts in the absence than in the presence of P15^{INK4b} expression. However, the levels of Cdk4-bound P16^{INK4a} do not increase upon TGF-β treatment, suggesting that P16^{INK4a} is not mediating the inhibitory activity of TGF-β (Figure 5B). These results suggest that either the induction

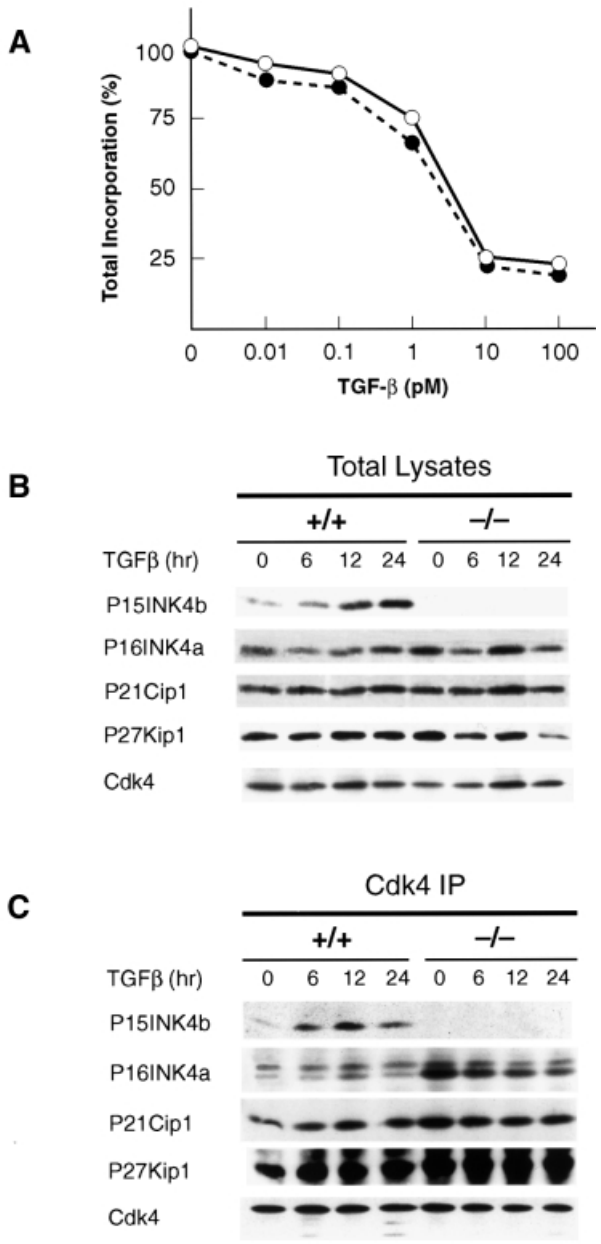

Fig. 5. Effect of TGF-β on mouse cells lacking P15^{INK4b}. (**A**) Inhibitory growth effect of TGF-β on cultured keratinocytes derived from wild-type (filled circles) or *P15*^{INK4b} (–/–) mice (open circles). Serial dilutions of TGF-β (0.01–100 pM range) were added to cells 5 days after plating. At 22 h after addition of TGF-β, cells were pulsed with [^{3}H]thymidine for 1 h. (**B**) Expression levels of P15^{INK4b}, P16^{INK4a}, P21^{Cip1} and P27^{Kip1} cell cycle inhibitory proteins in wild-type (+/+) and *P15*^{INK4b} (–/–)-deficient MEFs treated with TGF-β (100 pM) for the times indicated. (**C**) Levels of P15^{INK4b}, P16^{INK4a}, P21^{Cip1} and P27^{Kip1} proteins bound to Cdk4 in MEFs treated with TGF-β for the times indicated.

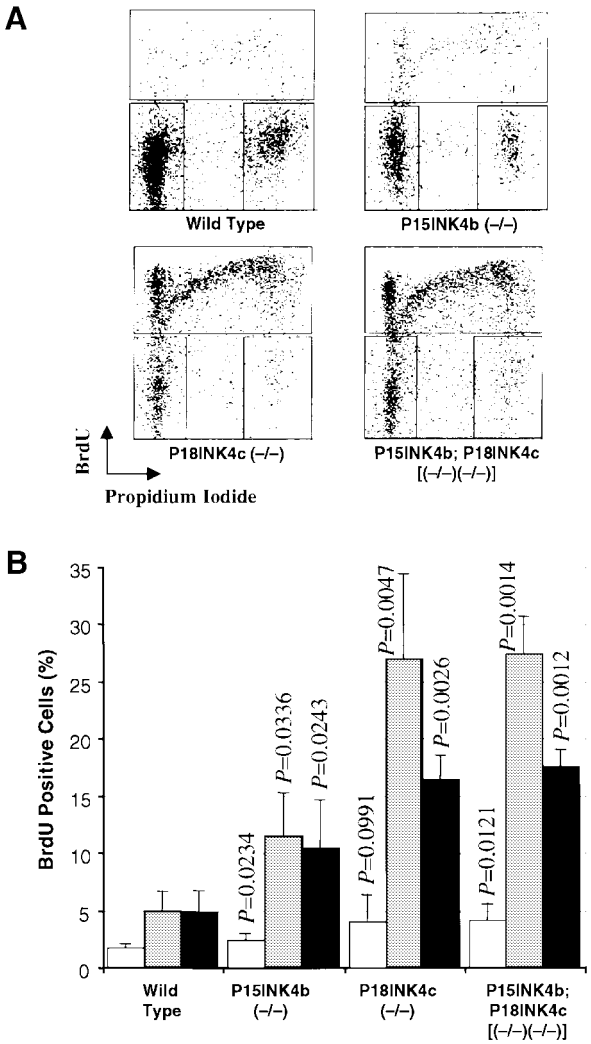

Fig. 6. Lymphocyte proliferation in P15^{INK4b} and P18^{INK4c} mutant mice. (**A**) Representative BrdU/propidium iodide plots showing lymphocyte activation after PMA + ionomycin treatment. (**B**) Bars show the average levels of BrdU incorporation and the standard deviation of duplicate experiments using cells from four different mice of each genotype untreated (open bars) or treated with PMA + ionomycin (shaded bars) or concanavalin A (filled bars). The proliferation of the mutant lymphocytes was compared with that of wild-type cells with identical treatment using the Student *t*-test.

of P15^{INK4b} is not responsible, at least completely, for the inhibitory growth effect of TGF-β, or that in the absence of this cell cycle inhibitor, TGF-β utilizes alternative pathways to induce cell cycle arrest.

Lymphocyte proliferation in P15^{INK4b} and P18^{INK4c} targeted mice

The lack of increased proliferative properties of P18^{INK4c}-defective MEFs contrasts with the results of an earlier report by Franklin *et al.* (1998) indicating increased proliferative properties of *P18*^{INK4c} (–/–) T and B lymphocytes upon mitogenic stimulation. To resolve this issue, we incubated primary spleen cells from either wild-type, *P15*^{INK4b} (–/–), *P18*^{INK4c} (–/–) or *p15*^{INKb};*P18*^{INK4c} [(–/–);(–/–)] with either concanavalin A or a mixture of phorbol 12-myristate 13-acetate (PMA) plus ionomycin. As illustrated in Figure 6, cultures derived from mice lacking either P15^{INK4b} or P18^{INK4c} expression display an increase in the number of cells entering the cell cycle. These results indicate that unlike MEFs, proliferation of spleen cells is controlled by both P15^{INK4b} and P18^{INK4c} proteins. However, spleen cells derived from double mutant mice did not show any significant increase in their response to mitogenic agents when compared with p18^{INK4c}-deficient lymphocytes. These results suggest that

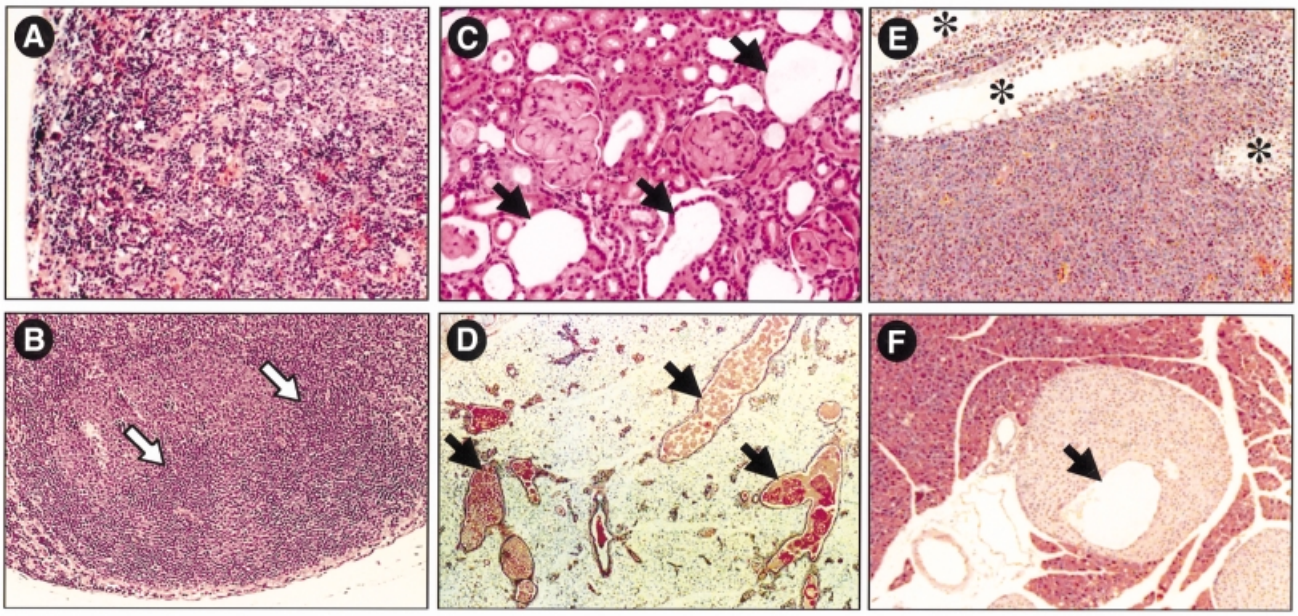

Fig. 7. Representative phenotypic abnormalities of *P15^{INK4b}* (–/–), *P18^{INK4c}* (–/–) and *P15^{INK4b};P18^{INK4c}* [(–/–);(–/–)] mutant mice. (**A** and **B**) *P15^{INK4b}* (–/–) mice. Histological analysis of (A) extramedullar hematopoiesis in the spleen and (B) secondary follicles in mesenteric lymph nodes of 12-week-old *P15^{INK4b}* null animals. (**C** and **D**) *P18^{INK4c}* (–/–) mice. Histological analysis of cysts (C) in the cortical region of the kidney and (D) in the galactophor ducts of the mammary epithelium of 12-week-old *P18^{INK4b}* null animals. (**E** and **F**) *P15^{INK4b};P18^{INK4c}* [(–/–);(–/–)] mice. Histological analysis of (E) a Leydig cell tumor of a 12-month-old mouse and (F) hyperplasia and cysts in pancreatic Langerhans islets of a 14-month-old mouse. None of these abnormalities were found in any of the wild-type mice examined. Arrows indicate the presence of (B) secondary germinal centers and (C, D and F) cystic structures. (E) Asterisks indicate residual seminiferous tubes. Original magnification is 100× (A, B and F), 200× (C) and 50× (D and E).

Table I. Tumor formation in *P15^{INK4b}* (–/–) mice

Genotype	No. of mice	No. of deaths	Mice with tumors	Histology[a]	Dead at (months)
(+/+)	42	4 (9%)	1 (2.4%)	lung adenoma (1)	16
(+/–)	100	6 (6%)	1 (1.0%)	sarcoma (1)	16
(–/–)	134	32 (24%)	11 (8.2%)	angiosarcoma[b] (7)	11–13
				skin fibrosarcoma (1)	13
				lung adenocarcinoma (1)	14
				pancreatic adenocarcinoma (1)	12
				lymphoma (1)	12

[a]The number of tumors observed is indicated in parentheses.
[b]Confirmed by positive staining for factor VIII (von Willebrand).

P15^{INK4b} and P18^{INK4c} play limited compensatory roles in controlling the proliferation of primary spleen cells.

Hematopoietic abnormalities in P15^{INK4b}- and P18^{INK4c}-null mice

Examination of *P15^{INK4b}* (–/–) mice at 2, 6 and 9 months of age revealed extramedullary hematopoiesis (EMH) and lymphoid hyperplasia in the spleen, and reactive lymph nodes characterized by prominent secondary follicles (Figure 7A and B). These pathologies are characterized by enlarged germinal centers and/or marginal zones and a moderate increase in the number of mitotic figures.

Immunofluorescence staining and flow cytometric analysis of thymocytes from 2-month-old wild-type and mutant mice with anti-CD3, CD4, CD8, CD25 and Thy1.2 antibodies did not reveal significant alterations (data not shown). Similar results were obtained when we examined myeloid cells with anti-Mac-1 antibodies. However, when we performed similar analyses with anti-B220 and anti-IgD antibodies, we observed increased levels of mature B cells co-expressing these antigens in spleen and lymph nodes (data not shown) of the mutant mice. Analysis of early stages of B-cell differentiation with markers such as CD43, HSA and CD19 indicated that early B-cell development is not affected in the absence of P15^{INK4b} expression (data not shown). Examination of 17 *P15^{INK4b}* (–/–) mice that died between 9 and 18 months of age, for which we had no evidence of tumor formation (see Table I), revealed that 13 of them had severe EMH and lymph node hyperplasia (76% incidence).

Histological examination of *P18^{INK4c}* (–/–) mice also revealed frequent splenomegaly after 6 months of age. The observed splenomegaly appears to be a consequence of cellular expansion of the white pulp. Although in most cases the morphology of the lymphocytic precursor cells appears to be normal, a few *P18^{INK4c}* (–/–) mice show dysplastic morphologies and, occasionally, lymphomas (see below). Other common hematopoietic defects present

in *P18*^{INK4c} (–/–) mice include enlarged lymph nodes, hyperplastic germinal centers and cellular expansion of plasma cells in the medulla (data not shown). The lymphoproliferative expansion in these mice is observed most often in kidneys, lung, liver and salivary glands. Interestingly, our *P18*^{INK4c} (–/–) mice do not display significant morphological abnormalities in the thymus to those previously reported with an independent strain of *P18*^{INK4c} knockout mice (Franklin *et al*., 1998). Whether there are thymic defects in our very young *P18*^{INK4c} (–/–) animals remains to be determined.

Cyst formation in P18^{INK4c} *(–/–) mice*

Histological examination of *P18*^{INK4c} (–/–) mice revealed cortical glomerulopathies after 9 months of age in ~30% of the animals. These glomerulopathies are due to the presence of multiple irregular cysts in the proximal tubules (Figure 7C). Less frequently, we have observed atrophic glomeruli and so-called glomerular cysts. In addition, female *P18*^{INK4c} (–/–) mice display mammary gland hyperplasia with ectasia in their galactophor ducts (Figure 7D). Often, these malformations in kidney and mammary tissue appear in the same animals.

Tumor susceptibility of P15^{INK4b} *(–/–) and P18*^{INK4c} *(–/–) mice*

To assess whether ablation of the *P15*^{INK4b} locus resulted in increased tumorigenesis, we aged 42 wild-type, 100 heterozygous and 134 homozygous mice and carefully monitored tumor development for up to 18 months. During this period of time, we only observed the appearance of tumors in 11 *P15*^{INK4b} (–/–) mice (8.2% incidence) versus one tumored mouse in each of the wild-type and heterozygous cohorts (2.4 and 1% incidence, respectively) (Table I). These results indicate that P15^{INK4b} has limited tumor-suppressing activities. The observed tumors had distinct pathologies. However, the most common type of neoplasia observed were tumors of connective tissue origin (eight out of 11; 73%) including seven angiosarcomas and one skin fibrosarcoma (Table I). Two other tumors were adenocarcinomas of the lung and pancreas (Table I). Finally, only one tumor was diagnosed as a lymphoma, characterized by a homogeneous population of abnormal cells, and the loss of normal architecture structures, including germinal centers and marginal zones. The low incidence of lymphomas adds further support to the concept that the EMH and lymph node hyperplasia observed in *P15*^{INK4b} (–/–) mice do not represent pre-neoplastic stages.

The susceptibility of *P15*^{INK4b} (–/–) mice to tumor formation was also investigated using a carcinogenic protocol similar to that used to test tumor susceptibility in mice lacking the *INK4a* locus (Serrano *et al*., 1996). Twenty-two wild-type, 39 *P15*^{INK4b} (+/–) and 22 *P15*^{INK4b} (–/–) mice were exposed to a single dose of 9,10-dimethyl-1,2-benzanthracene (DMBA) followed by repeated exposures to ultraviolet B rays (UVB). None of the mice treated developed detectable tumors and only one mouse from each group developed epidermal papillomas during a 12 month observation period. These results suggest that loss of P15^{INK4b} does not confer increased sensitivity to carcinogenic exposure.

In agreement with a previous report (Franklin *et al*., 1998), *P18*^{INK4c} (–/–) mice develop pituitary hyperplasia. About 40% of our *P18*^{INK4c} (–/–) mice (36 out of 91 animals) died before 18 months of age due to the presence of large pituitary tumors. None of their wild-type (109 mice) or heterozygous (53 mice) littermates had pituitary tumors. Pathological examination of these tumors indicated that most of them were chromophobe adenomas of the pars intermedia whereas one tumor was diagnosed as an adenoma of the adenohypophysis. These observations were confirmed by staining with specific markers including α-ACTH, α-MSH and α-LH antibodies (data not shown). These pituitary tumors did not show obvious signs of invasion into the brain and/or the spinal cord, and only in two cases could they be classified as carcinomas. Therefore, it is improbable that the cause of death of these mutant mice was due to the aggressiveness and/or metastatic potential of their pituitary tumors. Instead, it is likely that these tumors had fatally damaged critical structures of the nervous system since they were rather large, often 10 times the size of a normal pituitary gland. The development of these pituitary tumors is likely to be a slow process since *P18*^{INK4c} (–/–) mice display overt hyperplasia in their pituitary glands as early as 6 months of age (data not shown; Franklin *et al*., 1998).

A significant number of P18^{INK4c} mutant mice also develop other forms of neoplasia including testicular (seven out of 58 mice; 12% incidence) and adrenal gland tumors diagnosed as pheochromocytomas (six out of 58 mice; 10% incidence). We also observed other tumor types including B-cell lymphoma (two), angiosarcoma (two), thymic lymphoma (one) and renal cell carcinoma (one). These findings indicate that *P18*^{INK4c} has tumor suppressor properties in a variety of tissues. Moreover, the limited incidence of lymphomas in these mice indicates that the higher proliferative rate of P18^{INK4c}-defective lymphocytes does not necessarily represent a pre-neoplastic state.

P15^{INK4b} *and P18*^{INK4c} *double mutant mice*

The P15^{INK4b} and P18^{INK4c} proteins are widely expressed in a variety of tissues (Zindy *et al*., 1997a). To determine the putative compensatory roles of these highly related proteins, we generated *P15*^{INK4b};*P18*^{INK4c} [(–/–);(–/–)] double mutant mice. Specifically, we aged 40 *P15*^{INK4b};*P18*^{INK4c} [(–/–);(–/–)] double mutant mice and subjected them to a careful histopathological analysis, either when the animals showed signs of disease or when they reached 14 months of age. As summarized in Table II, more than half (55%) of these double mutant mice developed lymphoproliferative disorders, including splenomegaly, EMH, lymph node hyperplasia and the formation of hyperplastic germinal centers. Yet these lymphoproliferative states develop with the same kinetics and are histologically similar to those observed in single mutant mice, suggesting that, at least in lymphocytes, the absence of both INK4 proteins does not result in a more advanced proliferative stage than the loss of each one of them separately.

Tumor formation in these double mutant mice follows a similar pattern to that found in *P18*^{INK4c} and *P15*^{INK4b} single mutant mice. For instance, we observed pituitary adenomas with an incidence rate and kinetics similar to those observed in P18^{INK4c} (–/–) mice. These mutant mice

Table II. Summary of pathologies observed in *P15*^{INK4b};*P18*^{INK4c} [(–/–);(–/–)] double mutant mice

Pathology	Incidence	Observed in	
		p15 KO	p18 KO
Lymphoproliferative disorders	22/40 (55.0%)	yes	yes
Pituitary adenomas of the pars intermedia	19/40 (47.5%)	no	yes
Enlarged testis with cysts	**9/24 (37.5%)**	**no**	**no**
Ectasia in mammary glands	3/16 (18.9%)	no	yes
Kidney abnormalities (tubular and glomerular cysts/atrophy)	7/40 (17.5%)	no	yes
Langerhans islet hyperplasia with cysts	**2/40 (5.0%)**	**no**	**no**
Hematopoietic tumors	2/40 (5.0%)	yes	yes
Testicular tumors	1/24 (4.0%)	no	yes
Pheochromocytomas	1/40 (2.5%)	no	yes

Those pathologies not observed in either *P15*^{INK4b} (–/–) or *P18*^{INK4c} (–/–) single mutant mice are indicated in bold.

also developed lymphoma and testicular (Leydig cell) tumors (Figure 7E). Other tumor types such as angiosarcomas appeared in double mutant mice allowed to age up to 18 months (data not shown). So far, we have not identified adenocarcinomas such as those observed in mice lacking P15^{INK4b} alone (Table I). Whether these results are due to the more limited size (about half) of the cohort of double mutant mice examined in this study or are a direct consequence of the concomitant absence of P18^{INK4c} protein remains to be determined.

P15^{INK4b};*P18*^{INK4c} [(–/–);(–/–)] double mutant mice do not appear to display pathologies distinct from those observed in the single knockout strains. However, these double mutant mice undergo a more widely spread formation of cysts. Whereas cysts in *P18*^{INK4c} (–/–) mice appear to be restricted to kidneys and mammary glands, the double mutant mice also develop cystic structures in testis and pancreas (Table II; Figure 7F). The testes of nine out of 24 *P15*^{INK4b};*P18*^{INK4c} [(–/–);(–/–)] animals (37.5% incidence) were grossly enlarged with severe dilatation of the tubules of the rete testis with adjacent atrophy of seminiferous tubes, a pathology highly reminiscent of human testicular dysplasia, a congenital malformation that is usually associated with kidney malformation. Interestingly, four of the nine mice showing testicular cysts also display epithelial cysts in the cortical region of their kidneys. Whether congenital human testicular dysplasia involves mutations that affect INK4 protein expression remains to be determined. The additional development of cysts and hyperplasia in the Langerhans islets appears to be a less frequent event since we have only observed this phenotype in two out of 40 double mutant mice (Table II). Although the cellular mechanisms leading to the formation of cysts is not well understood, our results suggest limited compensatory roles for P15^{INK4b} and P18^{INK4c} proteins in controlling the proliferation of certain subpopulations of epithelial cells (e.g. testis and pancreas).

Discussion

The functional basis for the existence of four highly related INK4 proteins has not been established. Although these proteins exhibit distinct expression patters, it is well known that many cell types co-express two or more of these proteins. Thus, the existence of four distinct INK4 proteins cannot be explained solely on the basis of mutually exclusive spatial or temporal expression patterns. The generation of gene-targeted mice carrying specific deletions in one or several of these genes is beginning to provide critical information to solve these questions (Serrano *et al*., 1996; Franklin *et al*., 1998; Zindy *et al*., 2000). In this study, we report the generation of three strains of mice lacking P15^{INK4b} and P18^{INK4c} proteins alone or in combination. These mice are viable, indicating that P15^{INK4b} and P18^{INK4c} are not necessary for normal embryonic development. Our results indicate that *P15*^{INK4b} is a weak tumor suppressor. Indeed, the limited frequency and long latency of the tumors developed by these mutant mice indicate that loss of P15^{INK4b} does not result in overt loss of cell cycle control. Instead, the frequent appearance of lymphoproliferative disorders in these mice suggests that P15^{INK4b} may act to control cellular homeostasis. This hypothesis may explain the increased cellularity observed in the spleen and other organs of P15^{INK4b} (–/–) mice as well as the formation of secondary follicles in the lymph nodes, events reminiscent of physiological responses to external insults (e.g. infection) that induce cell proliferation. Although we have not observed increased cellularity in other tissues, the development of tumors of epithelial and mesodermal origin in these mutant mice suggests that loss of control of homeostatic cell proliferation may also take place in other cell types.

Previous studies have indicated that TGF-β-mediated growth arrest results in the rapid induction (up to 30-fold) of P15^{INK4b} in human keratinocytes (Hannon and Beach, 1994). Our results utilizing P15^{INK4b}-defective keratinocytes and MEFs clearly establish that P15^{INK4b} is not a mandatory mediator of TGF-β responses. For instance, Iavarone and Massague (1997) have reported that in tumor cells which have lost the *INK4b* locus, TGF-β induces cell arrest by repressing Cdc25A, a tyrosine phosphatase known to activate Cdks. More recently, it has been reported that TGF-β induces cell growth arrest of human HepG2 hepatocellular carcinoma cells by inhibiting a Cdk2-activating kinase (Nagahara *et al*., 1999). The mechanism by which TGF-β induces arrest of cell proliferation in P15^{INK4b}-deficient cells remains to be determined. However, our results indicate that the absence of P15^{INK4b} is not compensated by increased levels of expression or increased association with Cdk4 of other

members of the INK4 or Cip/Kip families of cell cycle inhibitors.

Loss of P18^{INK4c} also leads to lymphoproliferative disorders. Moreover, lymphocytes lacking this protein have a higher rate of proliferation than wild-type lymphocytes when submitted to mitogenic stimuli (Franklin *et al*., 1998; this report). These observations, along with the larger size and widespread organomegaly observed in these mutant mice, are also in agreement with a role for this protein in controlling homeostasis. Indeed, the appearance of cysts in the cortical region of the kidneys of *P18^{INK4c}* (–/–) mice could be due to unscheduled proliferation of epithelial cells. Loss of P18^{INK4c} leads to a wider spectrum of tumors than previously reported (Franklin *et al*., 1998). In addition to pituitary tumors, we have observed the appearance of tumors of testicular and adrenal gland (pheochromocytomas) origin in a significant fraction of *P18^{INK4c}* (–/–) mice. Less frequently, these animals also develop tumors of lymphoid, connective and epithelial cell origin, thus adding further support to the concept that *P18^{INK4c}* is a tumor suppressor.

Concomitant loss of *P15^{INK4b}* and *P18^{INK4c}* does not result in the generation of additional pathologies. In fact, the lymphoproliferative disorders observed in the double mutant mice are very similar to those found in *P15^{INK4b}* and *P18^{INK4c}* null animals. Likewise, primary splenocytes lacking these INK4 proteins show a response to activating signals similar to that of lymphocytes lacking only P18^{INK4c}. These observations indicate that P15^{INK4b} and P18^{INK4c} may act on similar checkpoint controls but mediate their effect through independent pathways, possibly by blocking phosphorylation of different Cdk4/6 substrates. In any case, our results indicate that neither of these proteins plays a pivotal role in controlling cell proliferation, possibly due to the compensatory roles by the Cip/Kip family of cell cycle inhibitors. This possibility has already been illustrated in pituitary cells using double P18^{INK4c};P27^{Kip2} mutant mice, which develop pituitary adenomas with a much shorter latency than either parental strain (Franklin *et al*., 1998).

The only significant differences observed between the phenotypes displayed by single and double mutant mice relate to the widespread formation of cystic structures. Whereas P18^{INK4c} null mice only display cysts in their kidneys and mammary epithelium, double mutant animals also develop cystic structures in their testes and, less frequently, in pancreas. These results indicate that P15^{INK4b} may play a compensatory role in epithelial cells of only certain tissues. In any case, the differential incidence of tumors observed in P18^{INK4c} mutant mice in spite of the wide tissue distribution of this protein clearly illustrates that P18^{INK4c} does not have the same tumor suppressor activity in all cell types and tissues. In this regard, it is interesting to note that whereas P18^{INK4c} prevents tumor formation in testis, the absence of the highly related P19^{INK4d} protein leads to testicular atrophy with increased apoptosis of germ cells (Zindy *et al*., 2000). Ongoing studies aimed at generating double P18^{INK4c};P19^{INK4d} mutant mice (in collaboration with M.Roussel's group) should help to clarify the apparently opposing roles of these highly related proteins in testicular cells.

In MEFs, the roles of P15^{INK4b} and P18^{INK4c} are clearly different. Although loss of P15^{INK4b} is not sufficient to release these primary cells from their cell contact inhibitory constrains or bypass senescence, *P15^{INK4b}* (–/–) MEFs exhibit proliferative advantage and are susceptible to morphological transformation by *ras* oncogenes. In contrast, loss of P18^{INK4c} does not appear to confer any proliferative advantage to MEFs, with the exception of a slight increase in the percentage of cells capable of initiating S phase after serum starvation. Loss of P18^{INK4c} does not make MEFs susceptible to morphological transformation by H-*ras* and c-*myc* oncogenes. Yet ablation of the *P18^{INK4c}* locus increases the susceptibility of P15^{INK4b}-deficient MEFs to H-*ras* transformation in a fashion similar to that provided by co-transfection with an SV40-driven c-*myc* oncogene. These observations add further support for a distinct functional role of P15^{INK4b} and P18^{INK4c} proteins and suggest that P18^{INK4c} may play a role, either related to or downstream from the c-*myc* oncogene.

In summary, ablation of the *P15^{INK4b}* and *P18^{INK4c}* genes in embryonic stem (ES) cells has allowed us to establish a role for these genes in controlling homeostatic levels of cell proliferation *in vivo* and to illustrate their tumor-suppressing abilities, at least in certain tissues. In addition, these genetic studies suggest that these INK4 proteins may work in parallel but independent pathways to control cell proliferation. Additional *in vitro* work will be necessary to identify the ultimate targets responsible for the growth-inhibitory effects of these proteins.

Materials and methods

Generation of P15^{INK4b} mutant mice

The left arm of the *P15^{INK4b}* targeting vector, pEL14, was generated by subcloning a 3.3 kbp *Bam*HI DNA fragment of genomic 129/Sv DNA containing the first exon of the *P15^{INK4b}* gene into the *Bam*HI site of pPNT (Tybulewicz *et al*., 1991). *Bam*HI sites were blunted to eliminate the 3′ *Bam*HI site in the targeted allele (Figure 1). The right arm of pEL14 was generated by subcloning a 9 kbp *Xho*I–*Xba*I DNA fragment of genomic 129/Sv DNA encompassing sequences downstream of the second exon into the *Xho*I–*Xba*I site of pBluescript. The resulting plasmid (pEL9) was digested with *Xho*I and *Not*I and subcloned into the *Xho*I–*Not*I sites of pPNT (Figure 1A). pEL14 DNA was transfected into CJ7 ES cells as described (Joyner, 1993). G418^{R}/Gan^{R} ES cell clones were analyzed by Southern blot using a 0.9 kbp *Bam*HI DNA fragment (probe A) and a 1 kbp *Bam*HI–*Xba*I DNA fragment (probe B) derived from genomic 129/Sv DNA sequences as probes (Figure 1). G418^{R}/Gan^{R} ES cell clones carrying a targeted *P15^{INK4b}* allele were either microinjected into C57BL/6 mouse blastocysts (clone B266-3188) or aggregated with morula cells from ICR mice (clones B266-396). Chimeras derived from these clones transmitted the targeted allele when bred to wild-type C57BL/6 and ICR mice, respectively. These strains of *P15^{INK4b}* (–/–) mice exhibited similar characteristics. The work described in this study was carried out with mice derived from the B266-3188 clone (129/Sv and C57BL6 mixed background). Primers used for genotyping included those of the *P15^{INK4b}* second exon, (GTCATGATGATGGGCAGCG and CCGGAATTC-GCGTGCAGATACCTCGC) (wild-type allele; 273 bp) or from intron 1 (ATCCGAGTGCCTACACCTCCA) and the *neo* gene (GCTCCC-GATTCGCAGCGCAT) (targeted allele; 500 bp).

Generation of P18^{INK4c} mutant mice

The P18^{INK4c} targeting vector, pEL32, was generated by subcloning a 4 kbp *Not*I–*Eco*RI(blunt) DNA fragment of genomic 129/Sv DNA containing the first coding exon of the *P18^{INK4c}* gene into the *Not*I–*Xho*I(blunt) site of pPNT (right arm) and a 5 kbp *Eco*RI DNA fragment of genomic 129/Sv DNA encompassing sequences downstream of the second exon into the *Eco*RI site of pPNT (left arm) (Figure 2A). G418^{R}/Gan^{R} ES cell clones were analyzed by Southern blotting using as probes a

2.6 kbp *Hin*dIII–*Eco*RV DNA fragment (probe A) and a 1 kbp *Xba*I–*Not*I DNA fragment (probe B) derived from genomic 129/Sv DNA (Figure 2B). G418^R/Gan^R ES cell clones carrying a targeted *P18^{INK4c}* allele were either microinjected into C57BL/6 mouse blastocysts (clone B301-31) or aggregated with morula cells from ICR mice (clones B301-338) as indicated above. Both strains of *P18^{INK4c}* (–/–) mice exhibited similar characteristics. The work described here was carried out with mice derived from the B310-31 clone (129/Sv and C57BL6 mixed background). Primers CCGGAATTCGAATGACAGCAAAACCAG and AGCCATCAAATTTATTCATGTTGCAGG were used for genotyping the wild-type allele (480 bp), whereas primers CCATTCGACCACCA-AGCGAAACATC and CGGCCACAGTCGATGAATCC were used for genotyping the targeted allele (250 bp).

Mouse embryo fibroblasts

MEFs were obtained and cultured as described (Deng *et al*., 1995). For colony formation assays, 2000 cells were seeded on 10 cm plates in triplicate and incubated in Dulbecco's modified Eagle's medium (DMEM) supplemented with 10% fetal bovine serum (FBS). After 2 weeks in culture, plates were stained with methylene blue and colonies (>1.5 mm in diameter) were scored. To analyze entry into S phase, early passage MEFs (P2) were incubated with DMEM in the absence of serum for 48 h. Cultures were induced to enter the cell cycle by the addition of DMEM supplemented with 10% FBS. BrdU was added at the times indicated (Figure 3C) at a final concentration of 10 μM for 2 h before harvesting the cells. BrdU incorporation was determined by using anti-BrdU–fluorescein isothiocyanate (FITC) antibodies (Pharmingen) and propidium iodide staining. Quantification of the percentage of BrdU-positive cells and DNA content was performed with the help of a Coulter-XL flow cytometer. For transfection assays, low passage MEFs (P2) were plated at a density of 10^6 cells per 10 cm dish in DMEM supplemented with 10% FBS. Saturating amounts of plasmid DNA (4–10 μg) supplemented up to 20 μg with carrier DNA were transfected following the standard calcium phosphate protocol (Graham and Van der Eb, 1973). The number of foci was scored 2 weeks after transfection.

Primary keratinocytes and TGF-β treatment

Primary mouse keratinocyte cultures were prepared from newborn mice as described (Glick *et al*., 1991). To assay the effect of TGF-β, cells were plated in 24-well plates at a density of 10^5 cells/well and maintained in low calcium (0.05%) Eagle's minimal essential medium supplemented with 8% dialyzed FBS (Hyclone) and 0.5% penicillin–streptomycin (Gibco-BRL) for 4 days. Serial dilutions of TGF-β (R&D Systems Inc.) were added in fresh medium and incubated for an additional 22 h. After this time, cells were labeled with 5 μCi/ml of [^{3}H]thymidine for 2 h. Labeled cells were harvested and the amount of label incorporated into DNA was determined using a Millipore vacuum filtration unit.

Immunoprecipitation and western blot analysis

MEFs were lysed in RIPA buffer and the lysates cleared by centrifugation at 14 000 r.p.m. for 10 min. For immunoprecipitation assays, lysates were incubated at 4°C for 2 h with antibodies elicited against Cdk4 (Santa Cruz Biotechnology) or P15^{INK4b}. Immunocomplexes were recovered by incubation with protein A–Sepharose beads (Pharmacia), and used for SDS–PAGE analysis. For immunoblot analysis, total cell extracts or immunoprecipitates were loaded onto a 15% SDS–polyacrylamide gel and subjected to electrophoresis. Electrophoresed proteins were transferred to an Immobilon membrane (Waters) and probed with antibodies. Immunocomplexes were visualized by enhanced chemiluminescence (Amersham) using goat anti-rabbit IgG antibodies coupled to horseradish peroxidase (Amersham). Antibodies to P16^{INK4a} and p27^{Kip1} were obtained from Santa Cruz Biotechnology. Antibodies against p21^{Cip1} were obtained from Pharmingen. Anti-P15^{INK4b} and P18^{INK4c} antibodies were raised against glutathione *S*-transferase (GST)–P15^{INK4b} (amino acid residues 24–130) and GST–P18^{INK4c} (amino acid residues 43–167) fusion proteins, respectively, and affinity purified.

Primary splenocyte cultures

Spleens were surgically removed from four 6-month-old mice. Single-cell suspensions were prepared by squeezing the organs through sterile syringes in RPMI-1640 medium supplemented with 10% FBS. For *in vitro* proliferation assays, duplicate cultures containing 2×10^5 spleen cells were incubated in 200 μl of RPMI-1640 medium supplemented with 10% FBS in either the presence or absence of 10 μg/ml concanavalin A (Sigma) or 50 ng/ml PMA (Sigma) + 500 ng/ml of ionomycin (Sigma). After 3 days in culture, cells were pulsed with 10 μM BrdU for 8 h. Labeled cells were harvested and BrdU incorporation measured in a flow cytometer as indicated above.

Histological and flow cytometric analysis

Tissues were fixed in 10% buffered formalin, embedded in paraffin and sectioned at 5 μm thickness. Sections were stained with hematoxylin and eosin for histological analysis. For flow cytometry analysis, cells from spleen, thymus and lymph nodes were collected, washed and resuspended in phosphate-buffered saline containing 1% bovine serum albumin prior to staining with conjugated antibodies elicited against the following antigens: CD3, CD4, CD8, CD25, Thy 1.2, CD44, B220, IgD, IgM, HSA, Ter-119, Mac-1, Gr-1, F4/80, 7/4 and ICAM-1. Antibodies were obtained from Gibco-BRL or Pharmingen. Flow cytometry was performed on a FACScalibur flow cytometer (Becton-Dickinson) and 10 000 events were collected in each case.

Acknowledgements

We thank Ernesto de la Cueva, Carmen Gómez and María Isabel Muñoz for their expert technical assistence. E.L. was partially supported by the Ministerio de Educacion y Ciencia of Spain. R.S. and J.M. are supported by fellowships from the Instituto de Salud Carlos III and the Fondo de Investigación Sanitaria, respectively. The initial part of this work was carried out when E.L. and M.B. were at the Bristol-Myers Squibb Pharmaceutical Research Institute. This project was partially supported by a research grant from Pfizer, Inc.

References

Blain,S.W., Montalvo,E. and Massagué,J. (1997) Differential interaction of the cyclin-dependent kinase (Cdk) inhibitor p27^{Kip1} with cyclin A–Cdk2 and cyclin D2–Cdk4. *J. Biol. Chem.*, **272**, 25863–25872.

Cheng,M., Olivier,P., Diehl,J.A., Fero,M., Roussel,M.F., Roberts,J.M. and Sherr,C.J. (1999) The p21^{Cip1} and p27^{Kip1} CDK 'inhibitors' are essential activators of cyclin D-dependent kinases in murine fibroblasts. *EMBO J.*, **18**, 1571–1583.

Deng,C., Zhang,P., Harper,J.W., Elledge,S.J. and Leder,P. (1995) Mice lacking p21$^{CIP1/WAF1}$ undergo normal development, but are defective in G_1 checkpoint control. *Cell*, **82**, 675–684.

Franklin,D.S. and Xiong,Y. (1996) Induction of P18^{INK4c} and its predominant association with CDK4 and CDK6 during myogenic differentiation. *Mol. Biol. Cell*, **7**, 1587–1599.

Franklin,D.S., Godfrey,V.L., Lee,H., Kovalev,G.I., Schoonhoven,R., Chen-Kiang,S., Su,L. and Xiong,Y. (1998) CDK inhibitors p18^{INK4c} and p27^{Kip1} mediate two separate pathways to collaboratively suppress pituitary tumorigenesis. *Genes Dev.*, **12**, 2899–2911.

Glendening,J.M., Flores,J.F., Walker,G.J., Stone,S., Albino,A.P. and Fountain,J.W. (1995) Homozygous loss of the P15^{INK4b} gene (and not the p16^{INK4} gene) during tumor progression in a sporadic melanoma patient. *Cancer Res.*, **55**, 5531–5535.

Glick,A.B., Sporn,M.B. and Yuspa,S.H. (1991) Altered regulation of TGF-β1 and TGF-β in primary keratinocytes and papillomas expressing v-Ha-*ras*. *Mol. Carcinog.*, **4**, 210–219.

Graham,F.L., and Van der Eb,A.J. (1973) A new technique for the assay of infectivity of human adenovirus 5 DNA. *Virology*, **52**, 456–467.

Hannon,G.J. and Beach,D. (1994) P15^{INK4b} is a potential effector of TGF-β-induced cell cycle arrest. *Nature*, **371**, 257–261.

Hatta,Y., Spirin,K., Tasaka,T., Morosetti,R., Said,J.W., Yamada,Y., Tomonaga,M. and Koeffler,H.P. (1997) Analysis of p18^{INK4C} in adult T-cell leukaemia and non-Hodgkin's lymphoma. *Br. J. Haematol.*, **99**, 665–667.

Herman,J.G., Jen,J., Merlo,A. and Baylin,S.B. (1996) Hypermethylation-associated inactivation indicates a tumor suppressor role for P15^{INK4b}. *Cancer Res.*, **56**, 722–727.

Iavarone,A. and Massagué,J. (1997) Repression of the CDK activator Cdc25A and cell-cycle arrest by cytokine TGF-β in cells lacking the CDK inhibitor p15. *Nature*, **387**, 417–422.

Joyner,A.L. (1993) In Rickwood,D. and Hames,B.D. (eds), *Gene Targeting: A Practical Approach*. Oxford University Press, Oxford, UK.

LaBaer,J., Garret,M.D., Stevenson,L.F., Slingerland,J.M., Sandhu,C., Chou,H.S., Fattaey,A. and Harlow,E. (1997) New functional activities for the p21 family of CDK inhibitors. *Genes Dev.*, **11**, 847–862.

Lois,A.F., Cooper,L.T., Geng,Y., Nobori,T. and Carson,D. (1995) Expression of the p16 and p15 cyclin-dependent kinase inhibitors in

lymphocyte activation and neuronal differentiation. *Cancer Res.*, **55**, 4010–4013.

Malumbres,M., Perez de Castro,I., Santos,J., Melendez,B., Mangues,R., Serrano,M., Pellicer,A. and Fernandez-Piqueras,J. (1997) Inactivation of the cyclin-dependent kinase inhibitor P15^{INK4b} by deletion and *de novo* methylation with independence of P16^{INK4a} alterations in murine primary T-cell lymphomas. *Oncogene*, **14**, 1361–1370.

Miller,C.W., Aslo,A., Campbell,M.J., Kawamata,N., Lampkin,B.C. and Koeffler,H.P. (1996) Alterations of the p15, p16, and p18 genes in osteosarcoma. *Cancer Genet. Cytogenet.*, **86**, 136–142.

Morgan,D.O. (1995) Principles of CDK regulation. *Nature*, **374**, 131–134.

Morse,L., Chen,D., Franklin,D., Xiong,Y. and Chen-Kiang,S. (1997) Induction of cell cycle arrest and B cell terminal differentiation by CDK inhibitor p18(INK4c) and IL-6. *Immunity*, **6**, 47–56.

Nagahara,H., Ezhevsky,S.A., Vocero-Akbani,A.M., Kaldis,P., Solomon,M.J. and Dowdy,S.F. (1999) Transforming growth factor β targeted inactivation of cyclin e:cyclin-dependent kinase 2 (Cdk2) complexes by inhibition of cdk2 activating kinase activity. *Proc. Natl Acad. Sci. USA*, **96**, 14961–14966.

Otsuki,T., Jaffe,E.S., Wellmann,A., Kumar,S., Condron,K.S. and Raffeld,M. (1996) Absence of p18 mutations or deletions in lymphoid malignancies. *Leukemia*, **10**, 356–360.

Phelps,D.E. and Xiong,Y. (1998) Regulation of cyclin-dependent kinase 4 during adipogenesis involves switching of cyclin D subunits and concurrent binding of p18^{INK4c} and p27^{Kip1}. *Cell Growth Differ.*, **9**, 595–610.

Phelps,D.E., Hsiao,K.M., Li,Y., Hu,N., Franklin,D.S., Westphal,E., Lee,E.Y. and Xiong,Y. (1998) Coupled transcriptional and translational control of cyclin-dependent kinase inhibitor p18^{INK4c} expression during myogenesis. *Mol. Cell. Biol.*, **18**, 2334–2343.

Reynisdóttir,I., Polyak,K., IavaroneA. and Massagué,J. (1995) Kip/Cip and Ink4 Cdk inhibitors cooperate to induce cell cycle arest in response to TGF-β. *Genes Dev.*, **9**, 1831–1845.

Rusin,M.R. *et al.* (1996) Intragenic mutations of the p16(INK4a), p15(INK4b) and p18 genes in primary non-small-cell lung cancers. *Int. J. Cancer*, **65**, 734–739.

Serrano,M., Lee,H.-W., Chin,L., Cordon-Cardo,C., Beach,D. and DePinho,R.A. (1996) Role of the INK4a locus in tumor suppression. *Cell*, **85**, 27–37.

Sherr,C.J. and Roberts,J.M. (1999) CDK inhibitors: positive and negative regulators of G_1-phase progression. *Genes Dev.*, **13**, 1501–1512.

Soos,T.J. *et al.* (1996) Formation of p27–CDK complexes during the human mitotic cell cycle. *Cell Growth Differ.*, **7**, 135–146.

Stone,S., Dayananth,P., Jiang,P., Weaver-Feldhaus,J.M., Tavtigian,S.V., Cannon-Albright,L. and Kamb,A. (1995) Genomic structure, expression and mutational analysis of the P15 (MTS2) gene. *Oncogene*, **11**, 987–991.

Tybulewicz,V.L., Crawford,C.E., Jackson,P.K., Bronson,R.T. and Mulligan,R.C. (1991) Neonatal lethality and lymphopenia in mice with a homozygous disruption of the c-*abl* proto-oncogene. *Cell*, **65**, 1153–1163.

Wuarin,J. and Nurse,P. (1996) Regulating S phase: CDKs, licensing and proteolysis. *Cell*, **85**, 785–787.

Zhang,S., Ramsay,E.S. and Mock,B.A. (1998) *Cdkn2a*, the cyclin-dependent kinase inhibitor encoding p16^{INK4a} and p19^{ARF}, is a candidate for the plasmacytoma susceptibility locus, *Pctr1*. *Proc. Natl Acad. Sci. USA*, **95**, 2429–2434.

Zindy,F., Quelle,D.E., Roussel,M.F. and Sherr,C.J. (1997a) Expression of the p16^{INK4a} tumor suppressor versus other INK4 family members during mouse development and aging. *Oncogene*, **15**, 203–211.

Zindy,F., Soares,H., Herzog,K.H., Morgan,J., Sherr,C.J. and Roussel,M.F. (1997b) Expression of INK4 inhibitors of cyclin D-dependent kinases during mouse brain development. *Cell Growth Differ.*, **8**, 1139–1150.

Zindy,F., van Deursen,J., Grosveld,G., Sherr,C.J. and Roussel,M.F. (2000) INK4d-deficient mice are fertile despite testicular atrophy. *Mol. Cell. Biol.*, **20**, 372–378.

Received January 28, 2000; revised May 5, 2000; accepted May 9, 2000